SCIENCE CHINA
Earth Sciences

• RESEARCH PAPER •

July 2014 Vol.57 No.7: 1438–1451
doi: 10.1007/s11430-014-4865-9

Roles of forced and inertially unstable convection development in the onset process of Indian summer monsoon

WU GuoXiong[1] & LIU BoQi[1,2*]

[1] *State Key Laboratory of Numerical Modeling for Atmospheric Sciences and Geophysical Fluid Dynamics (LASG), Institute of Atmospheric Physics, Chinese Academy of Sciences, Beijing 100029, China;*
[2] *Key Laboratory of Meteorological Disaster of Ministry of Education (KLME), Nanjing University of Information Science and Technology, Nanjing 210044, China*

Received May 30, 2013; accepted November 4, 2013; published online May 6, 2014

The NCEP/NCAR R1 reanalysis data are employed to investigate the impact of forced and inertial instability in the lower troposphere over the Arabian Sea on the onset process of Indian summer monsoon (ISM), and to reveal the important role of zonal advection of zonal geostrophic momentum played in the forced unstable convection. Results show that during the ISM onset the zero absolute vorticity contour ($\eta = 0$) shifts northward due to the strong cross-equatorial pressure gradient in the lower troposphere over southern Arabian Sea. Thus a region with negative absolute vorticity is generated near the equator in the northern hemisphere, manifesting the evident free inertial instability. When a southerly passes through this region, under the influence of friction a lower convergence that facilitates the convection flourishing at the lower latitudes appears to the north of zero absolute vorticity contour. However, owing to such a traditional inertial instability, the convection is confined near the equator which does not have direct influence on the ISM onset. On the contrary in the region to the north of the zero absolute vorticity contour and to the south of the low pressure center near the surface, although the atmosphere there is inertially stable, the lower westerly jet can develop and bring on the apparent zonal advection of zonal geostrophic momentum. Both theoretical study and diagnosing analysis present that such a zonal advection of geostrophic momentum is closely associated with the zonal asymmetric distribution of meridional land-sea thermal contrast, which induces a convergence center near and further north of the westerly jet in the lower troposphere over the southwestern coast of the Indian Peninsula, providing a favorable lower circulation for the ISM onset. It illustrates that the development of convection over the Arabian Sea in late spring and early summer is not only due to the frictional inertial instability but also strongly affected by the zonal asymmetric distribution of land-sea thermal contrast. Moreover, before the ISM onset due to the eastward development of the South Asian High (SAH) in the upper troposphere, high potential vorticity is transported to the region over the Arabian Sea. Then a local trumpet-shaped stream field is generated to cause the evident upper divergence-pumping effect which favors the ISM onset. When the upper divergence is vertically coupled with the lower convergence resulted from the aforementioned forced unstable convection development near the southwestern coast of Indian Peninsula, the atmospheric baroclinic unstable development is stimulated and the ISM onset is triggered.

forced convection development, Indian summer monsoon onset, zonal advection of zonal geostrophic momentum, South Asian High

Citation: Wu G X, Liu B Q. 2014. Roles of forced and inertially unstable convection development in the onset process of Indian summer monsoon. Science China: Earth Sciences, 57: 1438−1451, doi: 10.1007/s11430-014-4865-9

*Corresponding author (email: lbq@lasg.iap.ac.cn)

The Asian monsoon, including the South Asian monsoon and East Asian monsoon, is the strongest monsoon system in the world. The Asian monsoon can be divided into the tropical monsoon, subtropical monsoon, and temperate monsoon according to the climate belt. The tropical monsoon is composed of the Indian monsoon, the Bay of Bengal (BOB) monsoon, the South China Sea (SCS) monsoon, and the northwestern Pacific monsoon (Lau et al., 2009). The onset and evolution of Asian summer monsoon is complicated and spectacular. The tropical summer monsoon builds up from early May over the BOB to early June over India, lasting for about 40 days. But the East Asian summer monsoon takes about 50 days, starting from South China in early June and subsequently propagating to the North China in middle July when the Meiyu along the Yangtze River basin ends. The Indian summer monsoon (ISM) is one of the most important members in the Asian summer monsoon region. Its onset and intra-seasonal oscillation are significant for the variability and forecast of both Meiyu over the Yangtze River valley and precipitation over North China in boreal summer (Liu and Ding, 2008a, 2008b). Therefore, it is significant to understand the ISM onset process and the relevant mechanism correctly for improving climate prediction and disaster prevention and mitigation in China.

The climatological onset time of ISM is around the end of May and the beginning of June. The ISM onset dates are similar, determined by different criteria with different meteorological elements, such as rainfall, wind and moisture, etc (Ananthakrishnan et al., 1968; Prasad et al., 2005; Taniguchi et al., 2006; Wang et al., 2009). Recently Mao et al. (2004, 2007) used the seasonal overturns of the meridional temperature gradient (MTG) in the upper troposphere to define the onset dates of Asian summer monsoon. This definition is useful for studying the interaction among different subsystems of the Asian summer monsoon. It was reported that the seasonal northward migration of the intertropical convergence zone (ITCZ) is associated with the ISM onset featured by the advancing of monsoon depression and rainfall from the equator to the north (Saha et al., 1980; Gadgil, 2003). In detail, the precipitation in the monsoon region (70°–110°E, 10°–30°N) increases with the strengthened cross-equatorial Somali flow, which accelerates the lower-level jet and enhances the southwesterly over the Arabian Sea. Simultaneously the ITCZ is moving northward, and the ISM trough is established (Saha, 2010). Thus the seasonal northward shifting of ITCZ is of great importance for the ISM onset and advancement. The numerical simulation performed by Krishnamurti et al. (1983) showed that in the boundary layer of the ISM region, the geostrophic balance and advection balance (i.e., air parcel acceleration) existed to the north and the south of ITCZ, respectively. Such acceleration of cross-equatorial Asian summer monsoon circulation over the southwestern Indian Peninsula may be linked with the inertial instability. Tomas and Webster (1997) declared that the northward propagation of ITCZ over the ISM region is intimately correlated with the seasonal northward migration of near-equatorial zero absolute vorticity contour ($\eta = 0$) in the lower troposphere. It was presented that the negative absolute vorticity belt ($\eta < 0$) near the equator in the North Hemisphere (NH) reflects the inertial instability in the planet boundary layer (PBL). They also suggested that the criterion of inertial instability is $f \cdot \eta < 0$, in which f is the Coriolis parameter. If an air parcel passes northward through the inertially unstable ($f \cdot \eta < 0$) region, it will be accelerated under the inertial effect. When the air parcel passes through the inertial stable ($f \cdot \eta > 0$) area, it will be decelerated, forming a lower level convergence to the northern neighbor of the $\eta = 0$ contour. The northward migration of the zero absolute vorticity contour is caused by the increased cross-equatorial pressure gradient force associated with the intensified meridional gradient of sea surface pressure (SLP). Furthermore, Tomas et al. (1999) adopted an analytic method to demonstrate the possible dynamical mechanism for the near-equatorial inertial instability in boreal summer. They stressed the important influence of PBL drag coefficient (frictional effect) on the inertial instability, and successfully simulated the inertial instability and relative elements in the lower troposphere over the eastern Pacific and Atlantic Ocean in July by a simple one-dimensional PBL model. However, the simulation over the Indian Ocean is distinctly different from the observation. Then what's the reason for such a discrepancy? Dose the distribution of inertial instability in summer resemble that in spring? Given the close association between inertial instability and seasonal northward displacement of ITCZ in spring, is the theory of inertial instability applicable to the ISM onset from late spring to early summer in the NH? This paper aims to solve these scientific questions.

1 Data and methodology

1.1 Data description

The NCEP/NCAR R1 daily reanalysis dataset (1979–2009) with horizontal resolution of 2.5°×2.5° is utilized in this paper, including the wind, air temperature, geopotential height, specific humidity, and SLP fields (Kalnay et al., 1996). The wind, air temperature, and geopotential height fields are distributed on the 12 standard isobars from 1000 to 100 hPa, whereas the specific humidity field is on the 8 standard isobars from 1000 to 300 hPa. The daily outgoing longwave radiation (OLR) from 1979 to 2009 is supplied by NOAA (Liebmann and Smith, 1996). The daily precipitation observed by satellites (1997–2009) is from the Tropical Rainfall Measuring Mission (TRMM) offered by NASA (Huffman et al., 1995). The heat flux on the sea surface is attained from OAFlux datasets supported by the Woods

Hole Oceanographic Institution (WHOI, Yu et al., 2007).

1.2 Definition of ISM onset date

Following Mao et al. (2004), the ISM onset date is identified as the day when the following criteria are satisfied: (1) the area-averaged upper-tropospheric (500–200 hPa) MTG over the ISM region (60°–85°E, 10°–20°N) changes from negative to positive and (2) the MTG remains positive for more than 10 days. The ISM onset date defined by MTG criteria (Table 1) are similar to that by other methods (Prasad et al., 2005; Taniguchi et al., 2006; Xavier et al., 2007; Wang et al., 2009). To investigate the climatic features of inertial instability during the ISM onset accurately, the composite techniques based on the ISM onset date are adopted to remove the marked interannual variability of the ISM onset. For each individual year the onset date is defined as the zero date (D_0), with the dates before (after) the onset date being labeled as negative (positive) days. All the variables are chosen from –30 days (D_{-30}) to +30 days (D_{+30}) relative to the ISM onset date each year. The following analysis is all based on the composite results.

2 Dynamical characteristics of forced and inertially unstable convection development

Tomas et al. (1999) have examined the streamline field related with inertial instability by using a simple PBL model only forced by cross-equatorial pressure gradient. They adopted the homogeneous Helmhotz equation with frictional effect in PBL, but ignored other forcing in the inhomogeneous term. However, the cross-equatorial pressure gradient could lead to the lower jet and strong zonal advection over the tropical Arabian Sea in spring. As an air parcel moving eastward along the lower jet under the influence of pressure gradient force, its meridional speed is changed by the forcing of background pressure, affecting the spatial distribution of horizontal divergence and convection. Thus it is essential to consider the forcing of background pressure when studying the inertial instability issue over the ISM region. Here we start with deducing the control equation based on Tomas et al. (1999)'s framework. The 2-dimension control equation in PBL is:

$$\begin{cases} \dfrac{Du}{Dt} = fv - fv_{\mathrm{g}} - Ku = f(v - v_{\mathrm{g}}) - Ku, & (1) \\ \dfrac{Dv}{Dt} = -fu + fu_{\mathrm{g}} - Kv = -f(u - u_{\mathrm{g}}) - Kv, & (2) \end{cases}$$

in which $u_{\mathrm{g}} = -\dfrac{1}{f}\dfrac{\partial \phi}{\partial y}$ and $v_{\mathrm{g}} = \dfrac{1}{f}\dfrac{\partial \phi}{\partial x}$ are the zonal and meridional component of geostrophic wind, respectively; total derivative $\dfrac{D}{Dt} = \dfrac{\partial}{\partial t} + u\dfrac{\partial}{\partial x} + v\dfrac{\partial}{\partial y}$; and u, v, f, ϕ and K are respectively for the zonal wind, meridional wind, Coriolis parameter, geopotential, and the frictional coefficient. Before the ISM onset the strong cross-equatorial meridional gradient of sea surface temperature (SST) and sea level pressure (SLP) render the zonal geostrophic wind much larger than the meridional one over the Arabian Sea. We can thus assume $v_{\mathrm{g}} = \dfrac{1}{f}\dfrac{\partial \varphi}{\partial x} \approx 0$. Then eqs. (1) and (2) can be written as:

$$\frac{D^2 v}{Dt^2} + \lambda^2 v = f\left(u\frac{\partial u_{\mathrm{g}}}{\partial x} + \frac{\partial u_{\mathrm{g}}}{\partial t}\right) + Kf(2u - u_{\mathrm{g}}), \quad (3)$$

in which

$$\lambda^2 = f\eta - K^2,$$

and absolute vorticity

$$\eta = f - \frac{\partial u_{\mathrm{g}}}{\partial y}.$$

Eq. (3) is an atmospheric motion equation controlling the forced inertial movement. The RHS of eq. (3) is the inhomogeneous terms representing the external forcing. If the inhomogeneous terms are zero, eq. (3) will degenerate to an equation depicting the atmospheric free inertial oscillation with the following homogeneous solution:

$$v_0 = V\mathrm{e}^{i\lambda t}. \quad (4)$$

The inertial instability criteria are:

$$\lambda^2 = f\left(f - \frac{\partial u_{\mathrm{g}}}{\partial y}\right) - K^2 \begin{cases} < 0, & \text{unstable}, \\ = 0, & \text{neutral}, \\ > 0, & \text{stable}. \end{cases} \quad (5)$$

When the variations of u_{g} and u are much slower than

Table 1 ISM onset date[a)]

Year	Onset date	Year	Onset date
1979	June 5	1995	June 1
1980	June 1	1996	May 25
1981	May 27	1997	June 6
1982	May 30	1998	June 6
1983	June 13	1999	May 19
1984	May 24	2000	May 14
1985	May 23	2001	May 22
1986	June 1	2002	June 2
1987	June3	2003	June 1
1988	May 19	2004	May 9
1989	May 19	2005	May 30
1990	May 11	2006	May 20
1991	May 5	2007	June 2
1992	June 10	2008	June 3
1993	June 6	2009	May 19
1994	June 1	2010	May 23

a) average May 28

that of v, the particular solution of eq. (3) can be obtained as:

$$v^* = v_1^* + v_2^* = \lambda^2 \left[f\left(\frac{\partial u_g}{\partial t} + u\frac{\partial u_g}{\partial x} \right) + Kf(2u - u_g) \right], \quad (6)$$

in which,

$$v_1^* = \lambda^{-2} f\left(\frac{\partial u_g}{\partial t} + u\frac{\partial u_g}{\partial x} \right) = -\lambda^{-2}\left(\frac{\partial}{\partial t} + u\frac{\partial}{\partial x} \right)\left(\frac{\partial \phi}{\partial y} \right). \quad (7)$$

When $u_g = u_g(y)$,

$$v^* = v_2^* = \lambda^{-2} Kf(2u - u_g). \quad (8)$$

Eq. (7) indicates the influence on the meridional current passing through the isobars due to the zonal change in zonal geostrophic flow. Since the zonal geostrophic flow is proportional to the north-south pressure gradient, which is closely associated with the meridional land-sea thermal contrast, the particular solution v_1^* in eq. (7) thus implies that the zonal asymmetric distribution of north-south land-sea thermal contrast can affect the meridional motion of air parcel. In other words, the atmospheric inertial motion is also influenced by the external forcing of background streamline field. The solution v_2^* shown in eq. (8) indicates the effect of drag coefficient (friction) on the cross-isobaric meridional flow and inertial instability. Its dynamical connotation has been stressed in detail by Tomas et al. (1999). In this paper we concentrate on how the zonal variation of zonal geostrophic flow influences the meridional motion passing through the isobars, i.e., the particular solution v_1^*.

Traditionally inertial instability is applied to understand the development of convection in the ITCZ (Tomas and Webster, 1997; Tomas et al., 1999). To examine its effect on the ISM onset, a brief analysis is carried out on the near-equatorial stationary atmospheric motion by referring to Tomas et al. (1999)'s work. Then eqs. (1) and (2) can be predigested to:

$$\begin{cases} 0 = v\eta - Ku, & (9a) \\ 0 = -v\left(\dfrac{\partial v}{\partial y} + K \right) - \beta y u_{ag}. & (9b) \end{cases}$$

Note that the β-plane approximation $(f = \beta y)$ is adopted here and u_{ag} is the zonal ageostrophic wind. From late May to early June over the eastern Arabian Sea, a lower westerly jet is situated between 10°N and 15°N. The relative vorticity is negative to the south of the jet. Then the zero absolute vorticity contour is near 4°N. An inertially unstable ($\eta < 0$) region is located between the south of zero absolute vorticity contour and the equator, while the inertially stable ($\eta > 0$) area is located to the north of the zero absolute vorticity contour (Figure 1). Meanwhile the northward cross-equatorial gradient of SST leads to a high SLP in the south and a low one in the north of the Arabian Sea, corresponding to the zonal geostrophic flow near the equator. Near the equator the inertial force is small, and the pressure gradient force thus drives the air in the PBL to move northward crossing the equator from the southern hemisphere. The southerly passing through the inertial instability region forms an ageostrophic easterly to decelerate the westerly (eq. (9a)). Subsequently the southerly enters the inertially stable region and generates an ageostrophic westerly to accelerate the zonal eastward flow (eq. (9a)). Under the influence of inertial force, the zonal ageostrophic wind enhances the southerly crossing the isobars and the local meridional circulation gets intensified in the inertially unstable region, but weakens the southerly in the inertially stable area (eq. (9b)). In summary, in the inertial unstable region the southerly crossing the isobar is strengthened and the geostrophic westerly is weakened, whereas in the inertial stable region the southerly crossing the isobar gets damped and the geostrophic westerly is reinforced (Figure 1(a)). The quasi-equilibrium state of atmosphere requires the occurrence of divergence ($\partial v / \partial y > 0$) to the south but convergence ($\partial v / \partial y < 0$) to the north of the zero absolute vorticity contour in the lower troposphere (Figure 1(b), eq. (9b)). Therefore, the maximum of southerly occurs near the zero absolute vorticity contour and lower level convergence and convectional precipitation are produced to its north (Figure 1(c)).

The traditional theory of inertial instability described above can be applied to explain the frequent occurrence of convection along the ITCZ over the near-equatorial Arabian Sea before the ISM onset. But such convection is too far away from the Indian Peninsula to induce the ISM onset. Notice that the particular solution (v_1^*) is associated with both the zonal speed of air parcel and the zonal distribution of meridional pressure gradient, i.e., the influence of external forcing on the meridional motion. If the air parcel takes sufficient time to mix fully with the surrounding atmosphere as it moves eastward along the westerly, the individual variation of zonal geostrophic wind then will be proportional to the zonal gradient of zonal geostrophic westerly. Under such circumstances and based on eq. (7), over the area where the pressure gradient increases eastward, the northerly is accelerated in the inertial unstable region, while enhanced southerly appears to the north of zero absolute vorticity contour with its maximum occurring near the westerly jet axis. Thereby an additional forced convergence forms near or to the north of the zonal westerly maximum, and air ascent and convection are stimulated (Figure 1(d)). Since the lower westerly jet axis closing to the southwestern coast of Indian Peninsula is located near 10°–15°N over the Arabian Sea, such a forced convection development could affect the ISM onset more directly. In the next section the NCEP/NCAR R1 reanalysis data will be used to verify the impact of the forced convection development on the ISM

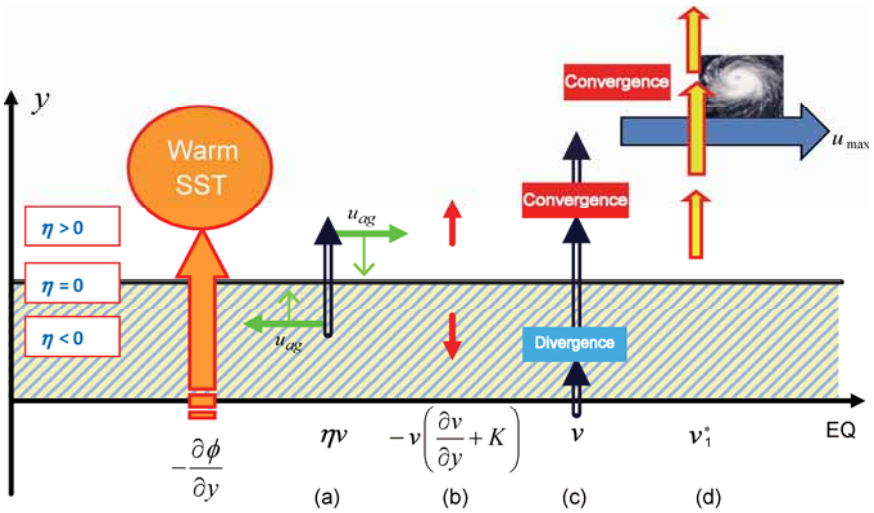

Figure 1 Schematic diagram of the forced and inertially unstable convection development. (a) Driven by the cross-equatorial sea surface pressure gradient force, when an air parcel passes through the inertially unstable region ($\eta < 0$)/inertially stable region ($\eta > 0$), the zonal wind is weakened/ strengthened (ηv , bold solid green arrows) and the southerly crossing the isobar gets increased/decreased ($-\beta y u_{ag}$, thin solid green arrows); (b) in order to balance the meridional inertial acceleration/deceleration induced by the zonal ageostrophic wind, the frictional and advection effects $(-v(\partial v/\partial y + K))$ have to decelerate/accelerate the southerly. (c) Thus the divergence/convergence is established to the south/north of the zero absolute vorticity contour. (d) Forced convection development: the zonal variation of meridional pressure gradient can generate strong additional meridional wind, and lower-layer convergence is produced near and to the north of the zonal wind maximum (u_{max}) which is located to the north of zero absolute vorticity contour, causing the forced convection development and leading to the ISM onset.

onset process.

3 Convection development during the ISM onset and relevant dynamical analysis

Figure 2 describes the evolution of precipitation and low level divergence during the ISM onset. Prior to the ISM onset the zero absolute vorticity contour stays to the south of 4°N, accompanied by the low-level convergence and rainfall center situated mainly between 10°N and the equator (Figure 2(a) to (c)). When the ISM onsets, the zero absolute vorticity contour shifts northward rapidly, so does the convergence in the lower troposphere. Then the strong lower convergence dominates the northern Arabian Sea, consistent with the evident rainfall migrating northward to the southwestern coast of Indian Peninsula (Figure 2(d)). After that the zero absolute vorticity contour maintains near 6°N, and the rainfall belt keeps advancing northward towards the Indian subcontinent (Figure 2(e) and (f)). During the whole onset period, there exists conspicuous divergence and negative absolute vorticity in the lower troposphere between the zero absolute vorticity contour and the equator in the NH. Generally, the precipitation is moving northward in the ISM onset process with the distinctly northward displacement of the zero absolute vorticity contour and convergence in the lower troposphere over the Arabian Sea. The northward shifting of zero absolute vorticity contour represents the strengthening of inertial instability *in situ*. According to the traditional theory of inertial instability (Tomas et al., 1999), the lower convergence should be located on the north side close to the zero absolute vorticity contour. However, the lower level convergence shown in Figure 2 is far away from the north edge of absolute vorticity zero contour, but close to the southwestern Indian Peninsula and the southeastern Arabian Sea, so that the traditional theory of inertial instability cannot explain such a phenomenon.

3.1 Effect of traditional inertial instability on the ISM onset

Figure 2 shows that the zero absolute vorticity contour moves northward most evidently in the region from 55°–65°E over the southern Arabian Sea. From the 55°–65°E averaged latitude-pressure cross section of the zero absolute vorticity contour (Figure 3(a)), it can be seen that the northward migration of the zero absolute vorticity contour over the Arabian Sea is restricted in the PBL under 700 hPa, resembling the results obtained by Tomas and Webster (1997). The reason for the northward movement of the zero absolute vorticity contour is the strong cross-equatorial gradient of SLP in the ISM region (Figure 3(b)). Before the ISM onset the enhanced poleward SLP gradient favors the intensifying and northward shifting of westerly jet, and pushes the zero absolute vorticity contour northward. Simultaneously, the pressure on the north of zero absolute vorticity contour decreases and the poleward gradient of SLP is enhanced, leading the zero contour to move towards the higher latitudes. It is due to this positive feedback that the zero absolute vorticity contour can move northward during

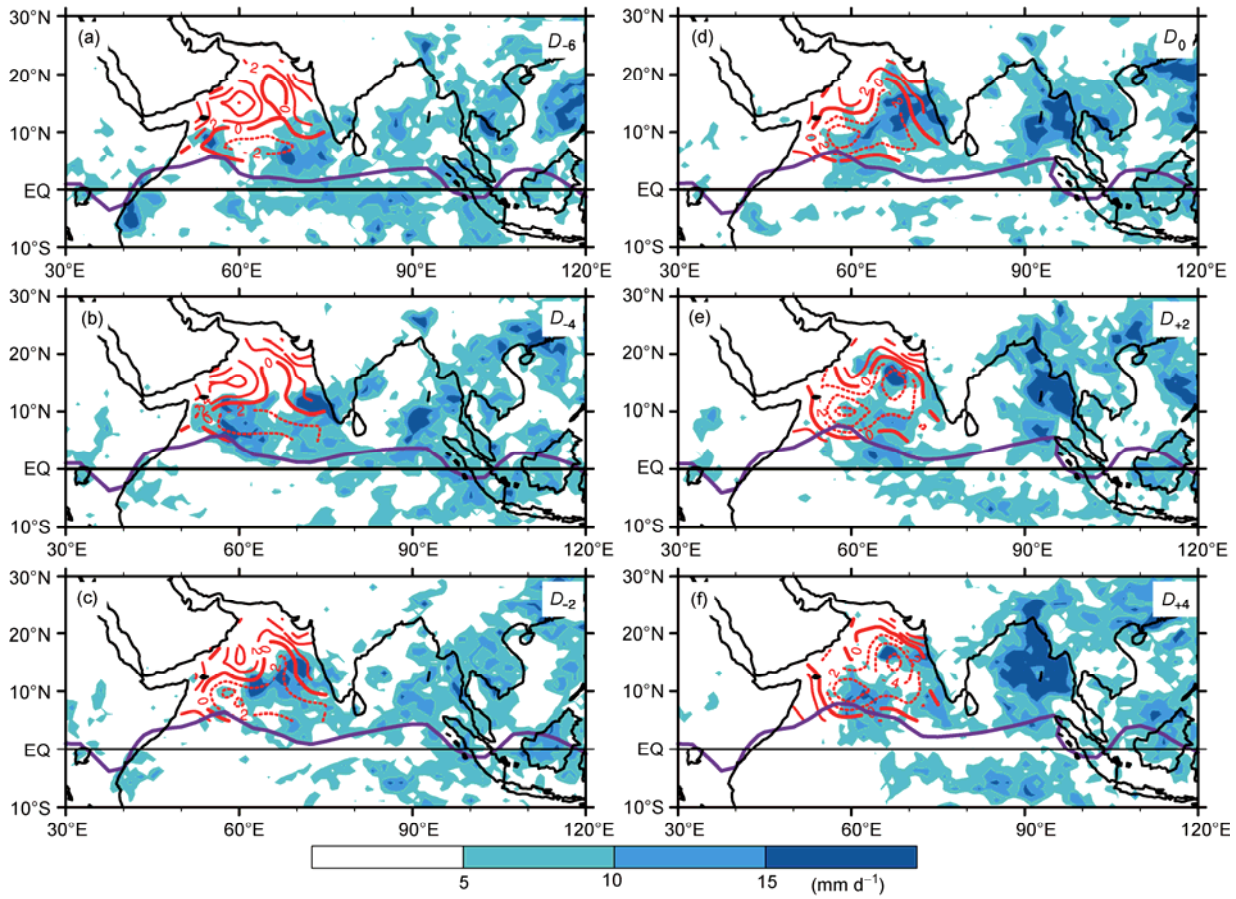

Figure 2 Evolution during the ISM onset of the TRMM precipitation (shading) and 925 hPa divergence (contours, dotted lines are for the convergence; interval is 2×10^{-6} s^{-1}).

the ISM onset. As latitude increases gradually the Coriolis parameter f is increasing, so that northward migration of the zero absolute vorticity contour stops at 6°N where $f > \zeta$ and the absolute vorticity becomes positive. Furthermore, the local SST over the Arabian Sea is high before the ISM onsets. After the ISM onsets, the summer monsoon engenders more cloud and rainfall to reduce the shortwave radiation reaching the sea surface and the enhanced sea surface wind stimulates the cold water upwelling and latent and sensible heat release. Thus the local SST is cooled quickly (Figure 3(c)). Consequently, the primary influence of traditional inertial instability on the ISM onset is manifested in the seasonal northward migration of ITCZ (Tomas and Webster, 1997; Gadgil, 2003), resulting in the reinforcement and northward movement of lower convergence near the equator only.

3.2 Influence on the ISM onset of forced convection development induced by zonal variation of meridional SLP gradient

The lower convergence caused by traditional inertial instability is too close to the equator to affect the ISM onset directly. Before the ISM onsets, as the cross-equatorial gradient of SLP gets strengthened, the zonal flow in the tropics is accelerated, generating a westerly jet in the lower troposphere over the southern Arabian Sea (Figure 4(a) to (c)). Then the enhanced lower level jet could increase the sensible heat flux on the sea surface, which facilitates the convection flourishing. After the ISM builds up, the convection cools the SST and decreases the sensible heating flux on the sea surface (Figure 4(d) to (f)). The convection and lower level convergence is intensified most rapidly over the southwestern Indian Peninsula, rather than the southwestern Arabian Sea where the zero absolute vorticity contour shifts northward most evidently. Given that the strong zonal momentum advection resulted from the lower westerly jet on the north of the zero absolute vorticity contour, it can be speculated that the external forcing should play an important role in the northward movement of convergence due to the forced convection development. In a steady state, the external forcing solution in eq. (7) can be written as:

$$v_1^* \approx \lambda^{-2} f\left(u\frac{\partial u_g}{\partial x}\right) = -\lambda^{-2}\left(u\frac{\partial}{\partial x}\right)\left(\frac{\partial \varphi}{\partial y}\right). \quad (10)$$

Figure 5 portrays the evolution of geopotential height at 925 hPa during the ISM onset. The zonal difference of low-level geopotential height is inconspicuous near the

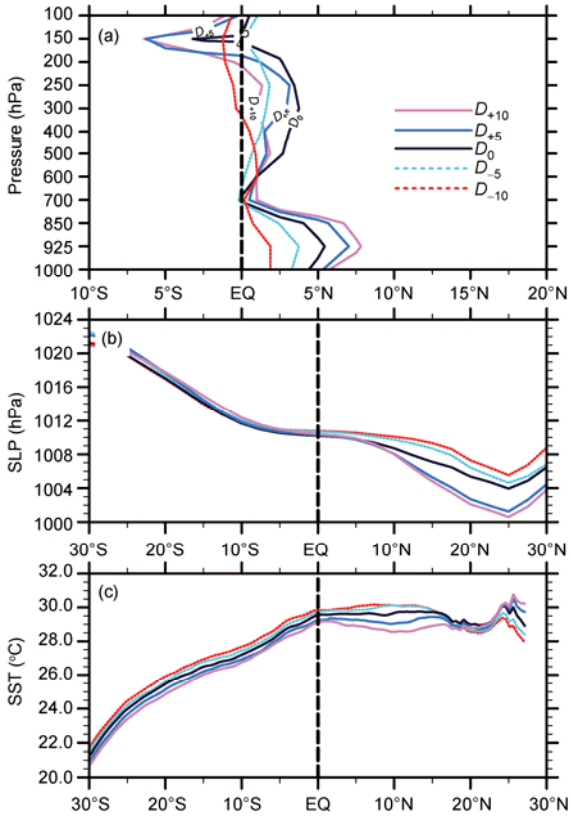

Figure 3 Evolution of 55°–65°E averaged vertical profile of zero absolute vorticity contour (a), and longitudinal profile of SLP (b), and SST (c).

equator. But to the north of 5°N, there is a high pressure over the Arabian Sea with a low one over the Indian Peninsula, making the meridional pressure gradient increase eastward over the eastern Arabian Sea from 5°N to 15°N. Based on eq. (10), the air parcel moving eastward along such a background pressure field should be driven to turn to the north, thereby producing an additional lower layer convergence to the north of the basic flow.

The evolvement of v_1^* at 925 hPa during the ISM onset is shown in Figure 6. The v_1^* over the eastern Arabian Sea is concentrated near the equator to the south of 6°N before the ISM onsets (Figure 6(a) to (c)). During the ISM onset process, however, the low-level westerly jet over the southern Arabian Sea accelerates and shifts northward because of the increasing cross-equatorial gradient of SLP. The westerly jet in the lower troposphere produces the zonal advection of zonal geostrophic momentum, which leads the most evident response of meridional wind to the east of 70°E, corresponding to the convergence near the southwestern coast of Indian Peninsula (Figure 6(d) to (f)). This strengthened low layer convergence in the NCEP/NCAR R1 reanalysis is in accordance with the intensified monsoon convection obtained from the TRMM satellite data as shown in Figure 2. It becomes evident that the zonal advection of zonal geostrophic momentum can force meridional wind to develop further downstream at higher latitudes, resulting in the low layer convergence and convection development over the

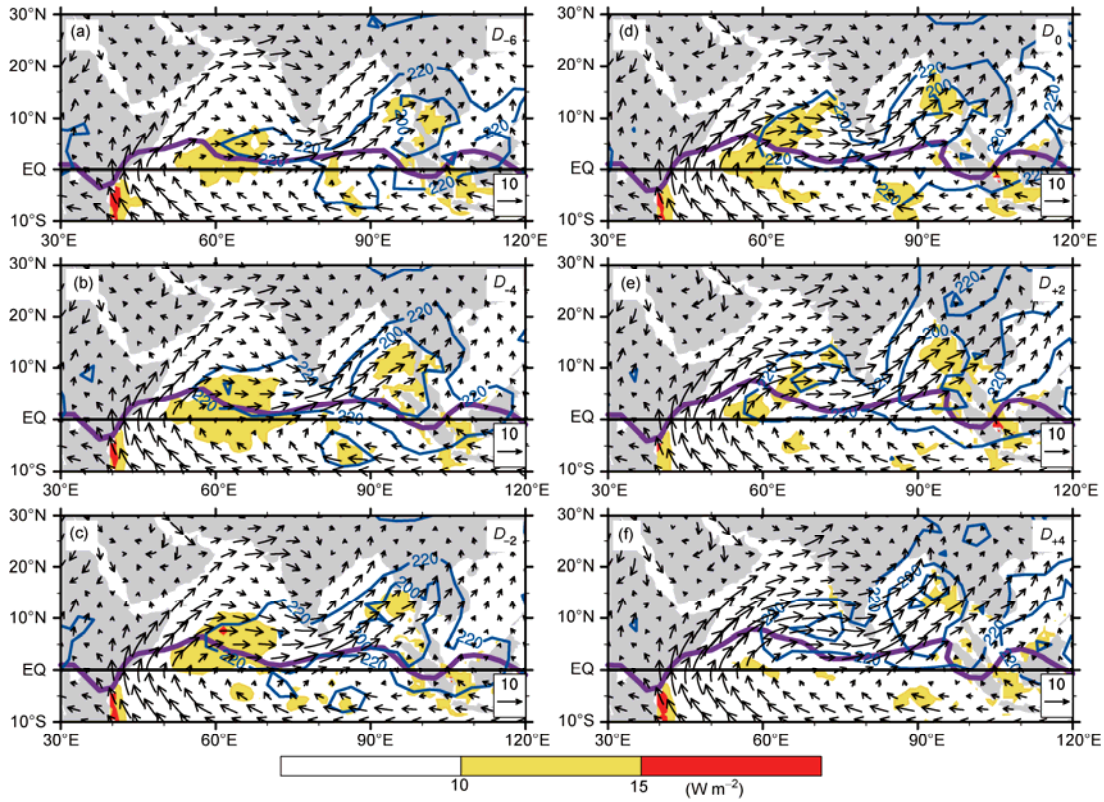

Figure 4 Evolution of sea surface sensible heating flux (shading), OLR (blue contours, unit: W m^{-2}) and 925 hPa wind (vectors, unit: m s^{-1}) during the ISM onset. The bold lines are for the zero absolute vorticity contours at 925 hPa.

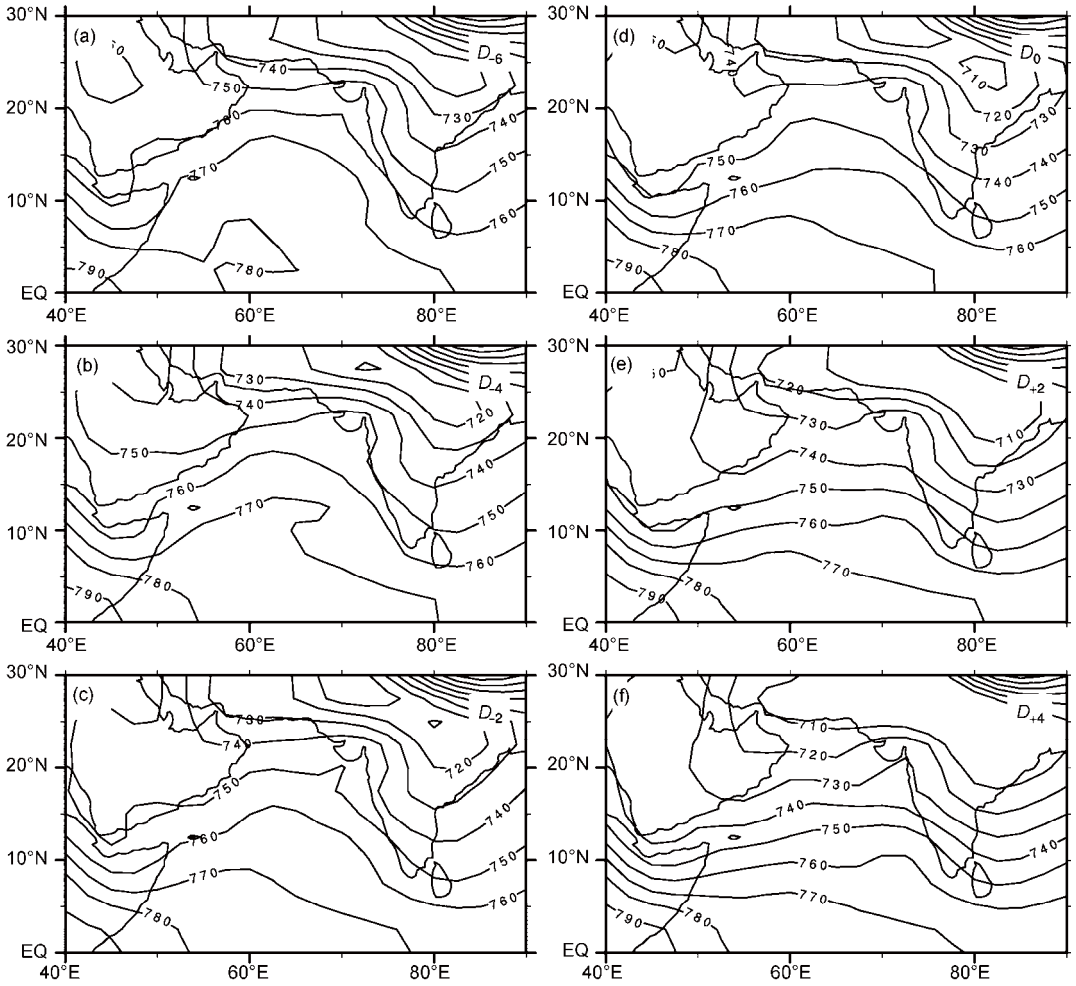

Figure 5 Evolution of 925 hPa geopotential height field (unit: gpm) during the ISM onset.

eastern Arabian Sea further away from the north edge of the zero absolute vorticity contour.

Briefly, the strengthened inertial instability during the ISM onset can affect the evolution of streamline field in the lower troposphere. The inertial instability over the Arabian Sea is characterized by the northward migration of the zero absolute vorticity contour due to the intensified cross-equatorial pressure gradient. Negative absolute vorticity appears near the equator in the NH. As the meridional current passing through this region, a dipole of southern divergence and northern convergence establishes straddling the zero absolute vorticity contour in the lower troposphere. Moreover, the cross-equatorial southerly enhances the zonal wind to the north of zero absolute vorticity contour, forming a low layer westerly jet over the tropical Arabian Sea. Because over the eastern Arabian Sea the north- south land-sea thermal contrast increases eastward, air parcel moving through this region along the lower westerly jet leads to strong zonal advection of zonal geostrophic momentum and deviates northward, causing the centers of convergence and convection formed to the north of jet axis in the lower troposphere over the southeastern Arabian Sea and the southwestern coast of Indian Peninsula to the east of 70°E. This forced convection development creates favorable conditions for the ISM onset.

4 Vertical coupling between upper and lower circulations during the ISM onset

4.1 Characteristics of the upper circulation

Except for the lower circulation, the contribution of the upper circulation to the ISM onset is also significant. Specifically, the SAH experiences evident variation during this period (Zhang et al., 2014; Liu et al., 2013). Prior to the ISM onset, the SAH situated over the Indochina Peninsula gets strengthened and expends eastward (Figure 7(a) to (c)) due to the monsoon convection over the BOB and SCS (Figure 4(a) to (c)). Then a conspicuous trumpet-shaped streamline field is established on its southwest just over the Arabian Sea, consistent with the strengthening of local divergence in the upper troposphere. During the ISM onset, the SAH expands further eastward and the upper divergence keeps intensifying over the Arabian Sea. According to

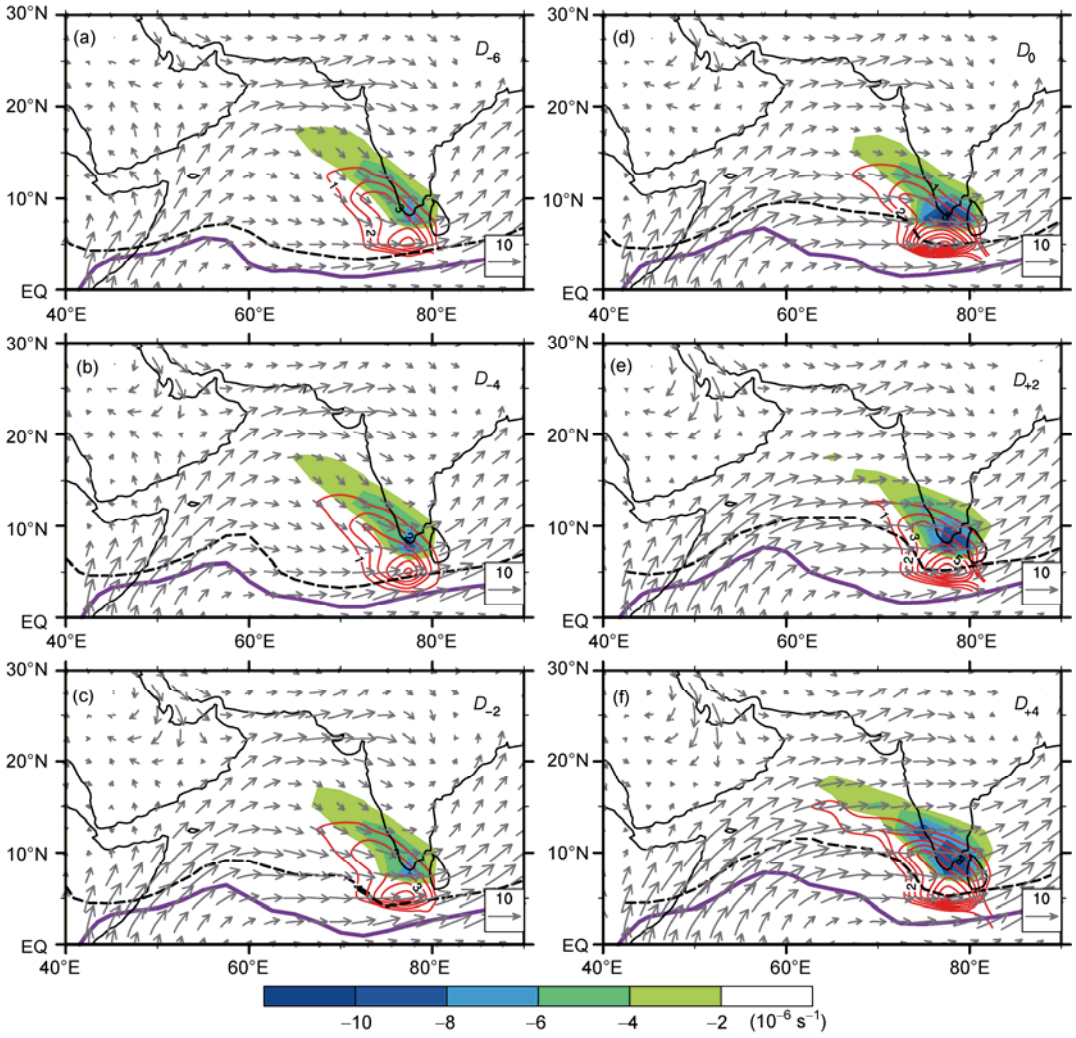

Figure 6 Evolution of the meridional wind $v_1^* \approx -\lambda^{-2}\left(u\frac{\partial}{\partial x}\right)\left(\frac{\partial \varphi}{\partial y}\right)$ (contours, unit: m s^{-1}) induced by forced convection development and its meridional convergence ($\partial v_1^*/\partial y$) at 925 hPa (shading). Vectors, purple solid lines and black dashed lines are for the winds (m s^{-1}), the zero absolute vorticity contour and the maximum axis of westerly at 925 hPa, respectively.

Zhang et al. (2014), the eastward expansion of the SAH enhances the northerly on its east, bringing high potential vorticity (PV) from mid-latitude southward to form a high PV belt. The high PV is then transported to the southwest of the SAH over the southern Arabian Sea by the easterly jet in the upper troposphere. Subsequently a local cyclonic curvature appears as a response to the high PV. The southeasterly of the cyclonic curvature, together with the northeasterly to its north, thus forms the trumpet-shaped streamline field on the southwest of the SAH, producing the upper divergence center, which supplies a favorite background of upper pumping to the ISM onset. Meanwhile the cross-equatorial pressure gradient pushes the zero absolute vorticity contour northward to accelerate the lower westerly jet, resulting in the lower convergence and convection to the east of 70°E near the southwestern coast of Indian Peninsula. Then how does the upper circulation couple with the lower system in vertical to influence the ISM onset?

4.2 Vertical coupling between the upper and lower circulations

According to the vorticity equation:

$$\frac{D(f+\zeta)}{Dt} = \left(\frac{\partial}{\partial t} + u\frac{\partial}{\partial x} + v\frac{\partial}{\partial y}\right)\cdot(f+\zeta) = f\frac{\partial w}{\partial z} \qquad (11)$$

at a steady state, $\frac{\partial}{\partial t} = 0$, assuming that w has normal mode solution in vertical, and taking partial derivative with respect to z on the both sides of eq. (11) leads to:

$$w \approx \frac{1}{f}\cdot\frac{\partial}{\partial z}(-\vec{V}\cdot\nabla(f+\zeta)). \qquad (12)$$

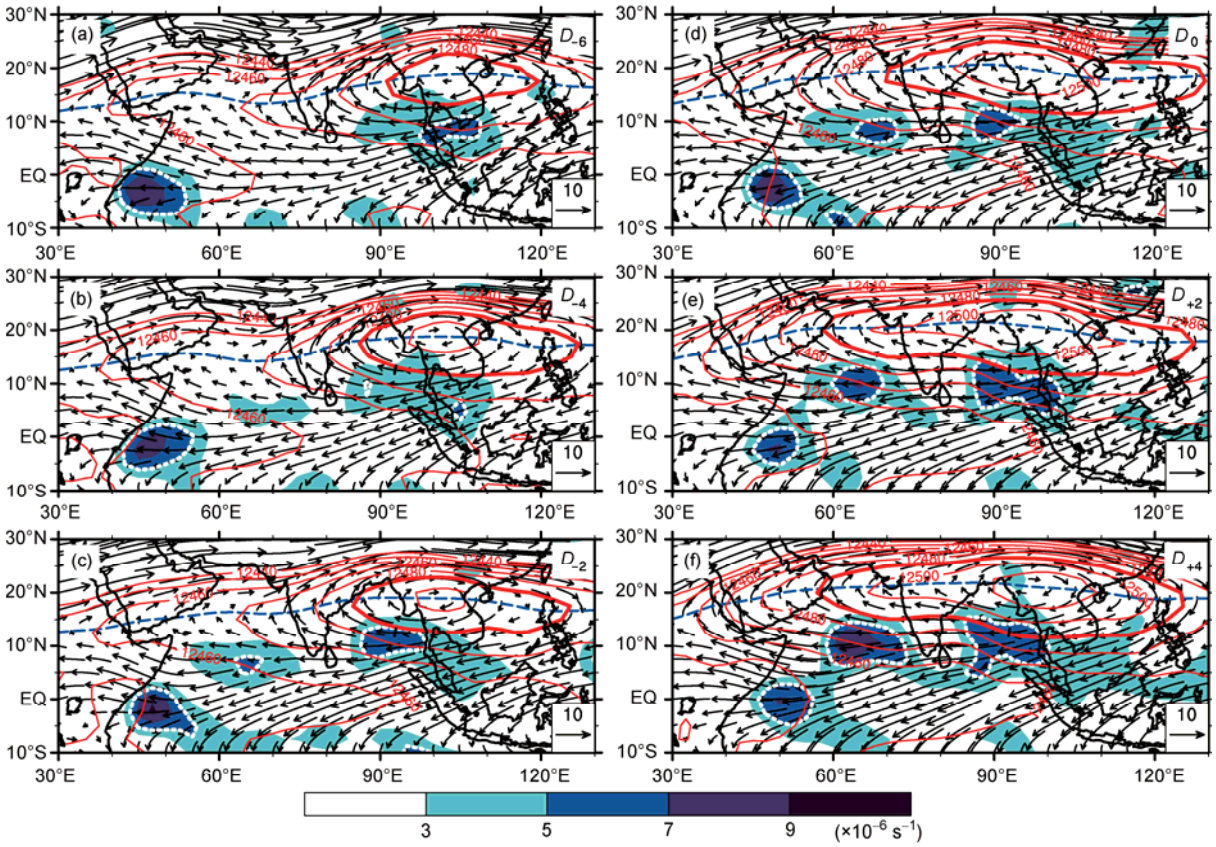

Figure 7 Evolution of wind (vectors, unit: m s^{-1}), geopotential height (contours, interval is 20 gpm) and divergence (shading, interval is 2×10^{-6} s^{-1}; white dotted lines are for the maximum of divergence) at 200 hPa during the ISM onset.

Eq. (12) delineates the effect of vertical shear of absolute vorticity advection on the vertical motion. That is, the ascending (descending) is accompanied by the advection of absolute vorticity increasing (decreasing) with height.

Figure 8 is the latitude-pressure cross section of vertical shear of absolute vorticity advection along 75°E during the ISM onset, indicating the favorite dynamical background for the ascending. As analyzed above, both the lower convergence and convection develop most rapidly along this longitude. Prior to the ISM onset, two near-equatorial ascending centers are located to the south of 5°N, including an upper center near 250 hPa and a lower one near 850 hPa (Figure 8(a) and (b)). On the D_{-2} the upper center stretches to about 10°N, but the lower center stays in place (Figure 8(c)). On the D_0, the upper center goes on enhancing with the development of lower center, so the vertical coupled ascending establishes from 5°N to 10°N. The collaboration of upper and lower centers promotes the ISM onset (Figure 8(d)). After that the upper center keeps expanding to the north of 10°N, while the lower center is still situated near 10°N. The divergence-pumping effect owing to the upper center facilitates the northward propagation of monsoon rainfall (Figure 7(e) and (f)). In fact, the upper center corresponds to the positive advection of absolute vorticity related with the high PV transport on the south of SAH, whereas the lower center is consistent with the northward migration of the zero absolute vorticity contour and the intensification of the forced convection development. In detail, when the SAH in the upper troposphere strengthens and elongates eastward, the high PV is transported to the southern Arabian Sea on D_{-2} (Figure 7(c)), the local upper divergence is enhanced, and the upper ascending center stretches northward (Figure 8(c)). Later, the northward shifting of the intensified divergence and ascending center aloft provide a background of upper pumping, stimulating the ISM onset and the northward advancing of the monsoon rainfall belt. In the lower troposphere, as the convergence associated with forced convection development and westerly jet begins to grow up near the southwestern coast of Indian Peninsula on D_0 (Figure 6(d)), the lower ascending center develops and migrates northward, and the ISM builds up (Figure 8(d)). Finally, the zero absolute vorticity contour moves further northward, and the lower convergence and monsoon rainfall also move to higher latitudes (Figure 8(e) and (f)), favoring the northward propagation of ISM.

The observed vertical motion exhibits similar features in both upper and lower troposphere (Figure 9) as those calculated and presented in Figure 8. Before the ISM onset, the two weak ascending centers are to the south of 5°N near the equator. The upper center is located at 250 hPa and and the lower center at 850 hPa. The descending is dominant to the north of 10°N (Figure 9(a)). Then the upper divergence-

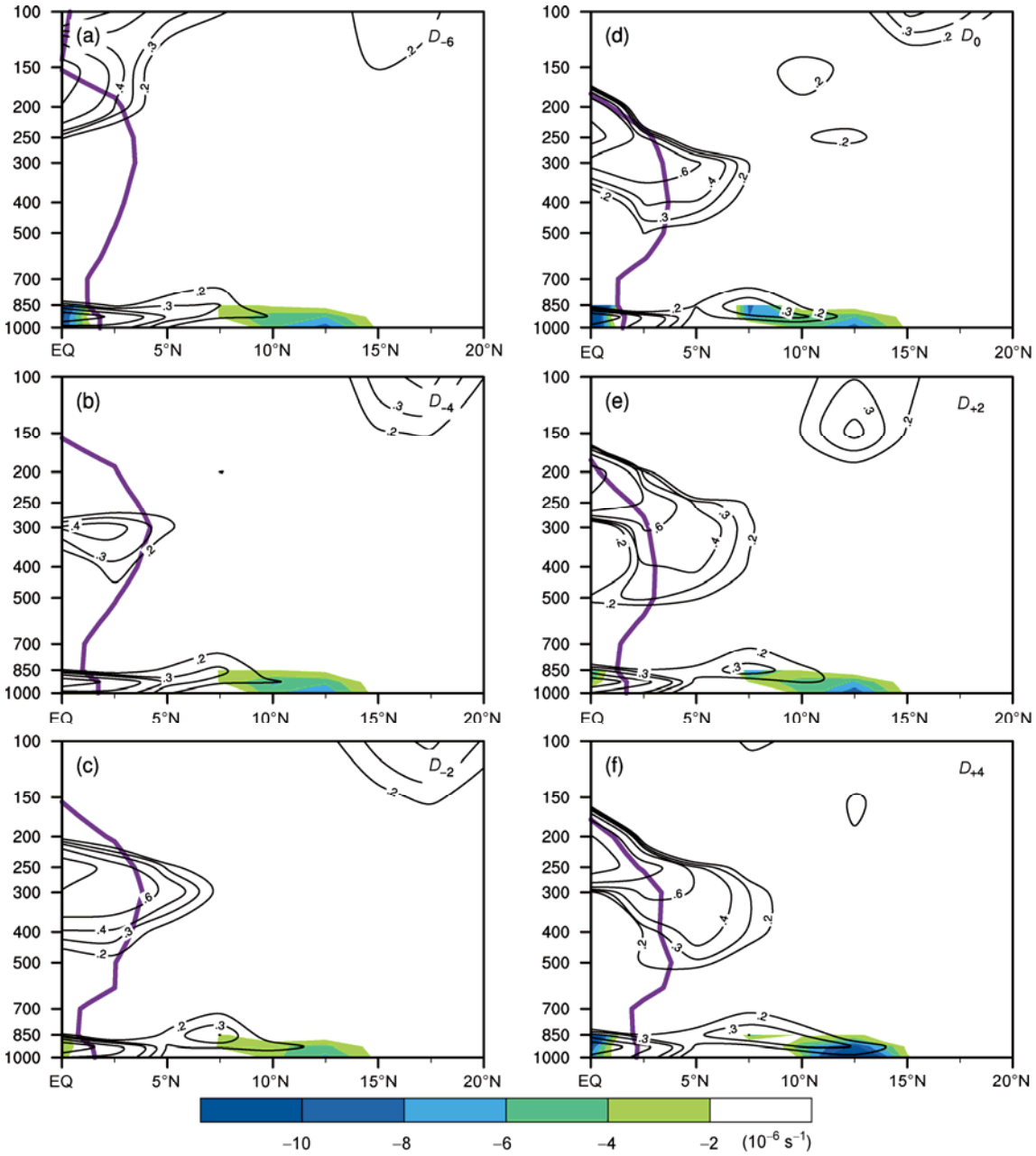

Figure 8 Evolution of pressure-latitude cross section along 75°E of the vertical shear of absolute vorticity advection $\left(-\frac{1}{f_0+\beta y}\cdot\frac{\partial}{\partial p}\left(-u\frac{\partial \zeta}{\partial x}-v\frac{\partial}{\partial y}(f+\zeta)\right), f_0=f\big|_{lat=2.5^\circ}\right)$ (contour, unit: 10^{-7} Pa^{-1} s^{-1}), and the meridional gradient of v_1^* ($\partial v_1^*/\partial y$) (shading). Bold solid purple lines are for the zero absolute vorticity contours along this longitude.

pumping effect is strengthened to enhance the upper ascending center above the southern Arabian Sea. Meanwhile the zero absolute vorticity contour and the lower ascending center both move northward, and the ascending center along the southwestern coast of Indian Peninsula starts to stretch to the north of 10°N (Figure 9(b) and (c)). When the ISM onsets, the strong pumping maintains in the upper troposphere, accompanied by the northward shifting of lower ascending center and monsoon rainfall (Figure 9(d)). The preliminary establishment of summer monsoon over the India is marked by the lower ascending center arriving at 10°N (Figure 9(e) and (f)). It is indicated that the observed ascending generally resembles the diagnosed one in the upper and lower troposphere by comparing Figure 8 with Figure 9. Therefore, the ascending stimulated by vertical shear of absolute vorticity advection is very important for the ISM onset. There exist some discrepancies between observation and diagnosis. First, due to the β-plane approximation in the

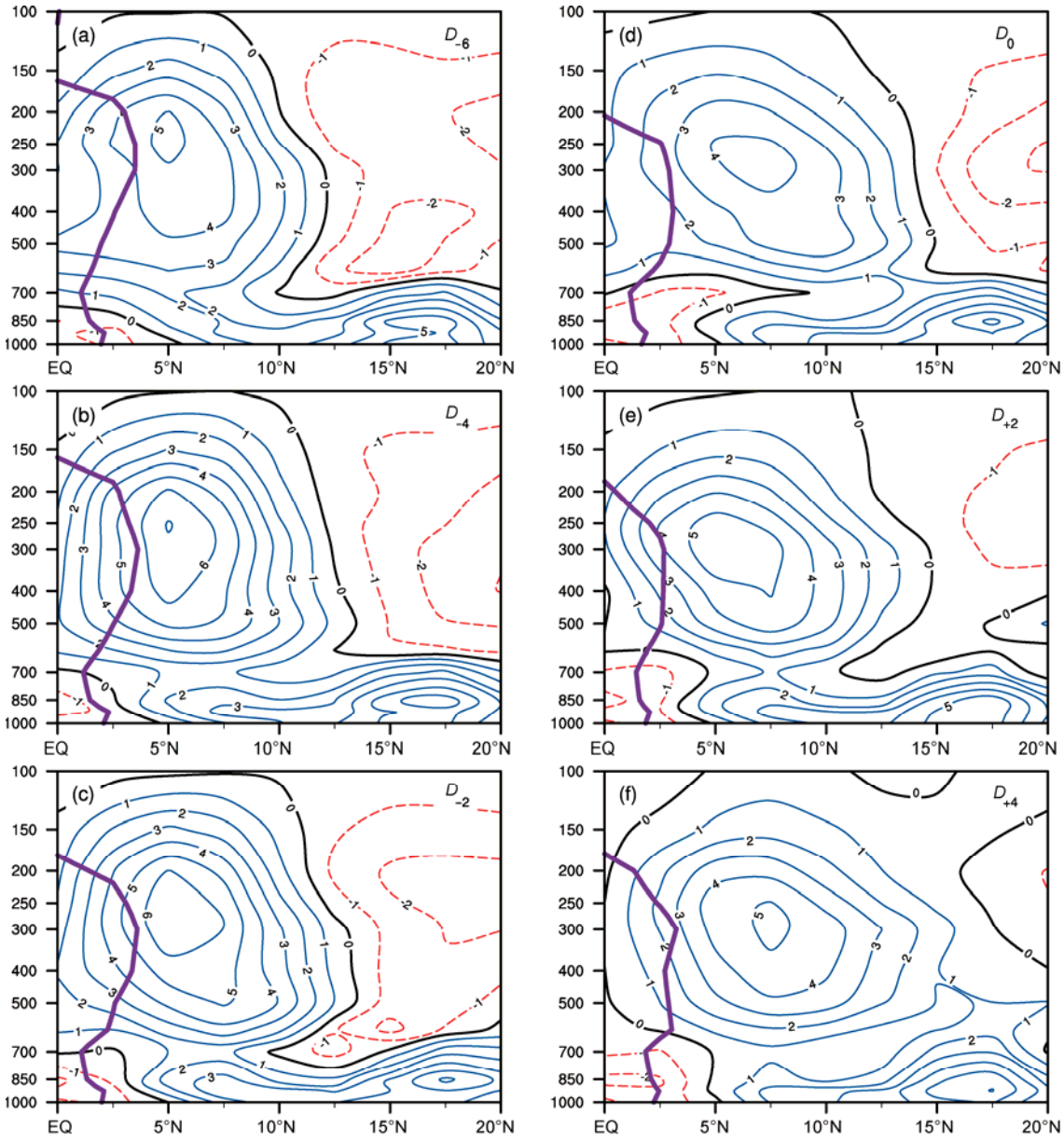

Figure 9 The same as Figure 8, but is about the vertical motion (10^{-2} Pa s^{-1}) obtained from the NCEP/NCAR R1 reanalysis.

diagnosis, the ascending is damped away from the equator, so the northward movement of low-level ascending in the diagnosis is weaker than that resulting from the observation. Besides, the apparent ascending of observation in the middle troposphere is not represented by the diagnosis. The reason is that only the ascending forced by internal dynamical process is contained in this diagnosis, while the ascending attributed to external thermal forcing (e.g., the condensation heating) is excluded.

Accordingly, before the ISM onset in the upper troposphere the SAH is enhanced and elongating eastward, and the high PV in the mid-latitude is transported to the southern Arabian Sea. Thus the local cyclonic curvature occurs on the southwest of SAH, and an upper trumpet-shaped streamline field with strong divergence is formed, providing pumping effect aloft and a favorable background for the ISM onset. In the lower troposphere, however, the convergence due to the forced convection development moves northward along the southwestern coast of Indian Peninsula. When the lower layer convergence is coupled with the upper layer divergence in vertical, the ascending in the ISM region is explosively intensified and heavy precipitation appears. Then the ISM builds up. Afterwards the ISM migrates northward gradually, manifested in the northward advancing of monsoon rainfall belt.

5 Discussion and summary

The ISM is an important member of the Asian monsoon

system, and its onset process reflects the abrupt circulation transition from winter to summer over South Asia. This paper uses the NCEP/NCAR R1 reanalysis datasets and the composite technology to investigate the climatological characteristics of ISM onset. The impact on the ISM onset of the frictional inertial instability in the lower troposphere is analyzed. It is highlighted that the zonal differential land-sea thermal contrast can induce low-level zonal advection of zonal geostrophic momentum and the resultant forced convection development is significant for the ISM onset. The importance of vertical coupling between upper and lower circulation during the ISM onset is also studied. The primary results are summarized as follows:

(1) The evident cross-equatorial pressure gradient exists in the PBL of Arabian Sea from late spring to early summer. It causes the zero absolute vorticity contour to move to the north from the equator, establishing a near-equatorial region with negative absolute vorticity in the NH. As the southerly passing through this region, the maximum of meridional wind takes place near the zero absolute vorticity contour, producing a dipole of southern divergence and northern convergence straddling the zero contour. Usually such a frictional instability occurs near the equator, and does not exert a direct impact on the ISM onset. On the other hand, the cross-equatorial pressure gradient generates a lower westerly jet over the southern Arabian Sea, and the zonal eastward increasing land-sea thermal contrast from the southeastern Arabian Sea to the southwestern Indian Peninsula produces a conspicuous local zonal advection of zonal geostrophic momentum. The advection induces a forced convection development with a low-level convergence located to the north of maximum westerly jet. Consequently the monsoon convection and heavy rainfall appear over the southeastern Arabian Sea and the southwestern coast of Indian Peninsula, marking the onset of ISM. Afterwards, as the forced convection development moving northward, the ISM precipitation advances northward over the Indian inland area.

(2) In addition to the forced convection development in the lower troposphere, the SAH evolution in the upper troposphere also plays a significant role in the ISM onset. Prior to the ISM onset, due to the latent heating released by the BOB and SCS monsoon, the SAH is strengthened and extends eastward. As a result the enhanced northerly on the east of the SAH brings the high PV from mid-latitude to the tropics, where the tropical easterly transports the high PV to the southern Arabian Sea in the upper troposphere. A local cyclonic curvature appears as a response to the high PV advection and forms, together with the cross equatorial northerly to the south, a trumpet-shaped streamline field on the southwest of the SAH, leading to stronger upper divergence-pumping. This provides another a background for the ISM onset. When the lower convergence moves northward below the upper divergence, the upper and lower circulation is fully coupled in vertical, the atmosphere becomes baroclinically unstable (Hoskins et al., 1985), and convection and severe rainfall develop near the southwestern coast of Indian Peninsula. Finally the ISM builds up.

This study demonstrates the climate mean features of the ISM onset, and sheds new light on the dynamic mechanism for further understanding the physical connotation of seasonal northward migration of monsoon rainfall belt over the ISM region. However, the interannual variability of ISM onset is so strong that the standard deviation of ISM onset date is about 9 days, implying the distinct difference of onset process from year to year (Joseph et al., 2006; Gadgil, 2011). The ISM onset time can be influenced by the ENSO events (Joseph et al., 1994; Goswami, 2005a), the condition of underlying surface and surrounding snow cover (Yang et al., 1996; Robock et al., 2003), the intraseasonal oscillation (Wu and Zhang, 1998; Goswami, 2005b), and the extra-tropical circulation anomalies (Chang et al., 2001). In particular, the effect of ENSO events is most prominent since it is a global scale forcing which persists from previous winter to concurrent summer. Joseph et al. (1994) proposes that the ISM onset is postponed after the occurrence of strong El Niño event in previous winter, which may induce the SST anomalies over the Indian Ocean and the Pacific. Fasullo and Webster (2003) use the vertically integrated water vapor transport to define the ISM onset date, and propose that there is a significant positive correlation between the ISM onset date and the Niño-3 SST anomalies averaged from June to September. Xavier et al. (2007) identify the ISM onset date based on the meridional difference of air temperature averaged in the upper troposphere to confirm its significant and steady positive correlation with the ENSO events. Nevertheless, previous studies concentrate mainly on the statistic relationship between ENSO events and ISM onset date, little investigation was done about the influence of ENSO on the ISM onset process and relevant mechanism, especially the effect on the circulation in the middle and upper troposphere. This paper highlights the important role of both the forced convection development in the lower troposphere and the SAH variation in the upper troposphere played in the ISM onset. To further understand the ISM onset process, more studies are required to examine the ENSO effect on the ISM onset via its influence on the dynamical processes revealed in this study.

This work was supported jointly by the CAS Programme (Grant No. XDA11010402), the National Basic Research Program of China (Grant Nos. 2010CB950403, 2012CB417203), the National Natural Science Foundation of China (Grant No. 41275088), and the Project founded by China Postdoctoral Science Foundation.

Ananthakrishnan R, Srinivasan V, Ramakrishna A R, et al. 1968. Synoptic features associated with onset of southwest monsoon over Kerala. Forcasting Manual, Vol IV-18.2, India Meteorological Department

Chang C P, Harr P, Ju J. 2001. Possible roles of Atlantic circulations on the weakening Indian monsoon rainfall-ENSO relationship. J Clim, 14: 2376–2380

Fasullo J, Webster P J. 2003. A hydrological definition of Indian Monsoon onset and withdrawal. J Clim, 16: 3200–3211
Gadgil S. 2003. The Indian monsoon and its variability. Ann Rev Earth Planet Sci, 31: 429–467
Gadgil S, Rajeevan M, Zubair L, et al. 2011. South Asian Monsoon: Interannual variation. In: Chang C P, Ding Y H, Lau N C, et al, eds. The Global Monsoon System: Research and Forecast (2nd). New York: World Scientific. 25–42
Goswami B N. 2005a. South Asian summer monsoon: An overview. In: Chang C P, Wang B, Lau N C, et al, eds. The Global Monsoon System: Research and forecast (2nd). New York: World Scientific. 47–71
Goswami B N. 2005b. South Asian monsoon. In: Lau K-M, Waliser D E, eds. Intraseasonal Variability in the Atmosphere-Ocean Climate System. London: Springer. 19–61
Huffman G J, Adler R F, Rudolf B, et al. 1995. Global precipitation estimates based on a technique for combining satellite-based estimates, rain gauge analysis, and NWP model precipitation information. J Clim, 8: 1284–1295
Joseph P V, Eischeid J K, Pyle R J. 1994. Interannual variability of the onset of the Indian summer monsoon and its association with atmospheric features, El Nino, and sea surface temperature anomalies. J Clim, 7: 81–105
Joseph P V, Sooraj K P, Rajan C K. 2006. The summer monsoon onset process over South Asia and an objective method for the date of monsoon onset over Kerala. Int J Climatol, 26: 1871–1893
Kalnay E, Kanamitsu M, Kistler R, et al. 1996. The NCEP/NCAR 40-Year Reanalysis Project. Bull Amer Meteorol Soc, 77: 437–471
Krishnamurti T N, Low-Nam S, Pasch R. 1983. Cumulus parameterization and rainfall rates II. Mon Weather Rev, 111: 816–828
Lau N-C, Ploshay J J. 2009. Simulation of synoptic and sub-synoptic scale phenomena associated with the East Asian Summer Monsoon using a high-resolution GCM. Mon Weather Rev, 137: 137–160
Liebmann B, Smith C A. 1996. Description of a complete (interpolated) Outgoing Longwave Radiation dataset. Bull Amer Meteorol Soc, 77: 1275–1277
Liu B Q, Wu G X, Mao J Y, et al. 2013. Genesis of the South Asian High and Its Impact on the Asian Summer Monsoon Onset. J Clim, 26: 2976–2991
Liu Y Y, Ding Y H. 2008a. Teleconnection between the Indian summer monsoon onset and the Meiyu over the Yangtze River Valley. Sci China Ser D-Earth Sci, 51: 1021–1035
Liu Y Y, Ding Y H. 2008b. Analysis and numerical simulations of the teleconnection between Indian summer monsoon and precipitation in North China. Acta Meteorol Sin, 22: 489–501
Mao J Y, Chan J C L, Wu G X. 2004. Relationship between the onset of the South China Sea summer monsoon and the structure of the Asian subtropical anticyclone. J Meteorol Soc Jpn, 82: 845–859
Mao J Y, Wu G X. 2007. Interannual variability in the onset of the summer monsoon over the Eastern Bay of Bengal. Theor Appl Climatol, 89: 155–170
Prasad V S, Hayashi T. 2005. Onset and withdrawal of Indian summer monsoon. Geophys Res Lett, 32: L20715, doi: 10.1029/2005GL023269
Robock A M, Mu M Q, Vinnikov K, et al. 2003. Land surface conditions over Eurasia and Indian summer monsoon rainfall. J Geophys Res, 108: 4131, doi: 10.1029/2002JD002286
Saha K. 2010. Chapter 4: Monsoon over Southern Asia (comprising Pakistan, India, Bangladesh, Myanmar and Countries of Southeastern Asia) and adjoining Indian Ocean (Region-I). In: Saha K, ed. Tropical Circulation Systems and Monsoons. London: Springer. 89–121
Saha S, Saha K. 1980. A hypothesis on onset, advance and withdrawal of the Indian Summer Monsoon. Pure Appl Geophys, 118: 1066–1075
Taniguchi K, Koike T. 2006. Comparision of definitions of Indian summer monsoon onset: Better representation of rapid transitions of atmospheric conditions. Geophys Res Lett, 33: L02709, doi: 10.1029/2005GL024526
Tomas R A, Webster P J. 1997. The role of inertial instability in determining the location and strength of near-equatorial convection. Q J R Meteorol Soc, 123: 1445–1482
Tomas R A, Holton J R, Webster P J. 1999. The influence of cross-equatorial pressure gradients on the location of near-equatorial convection. Q J R Meteorol Soc, 125: 1107–1127
Wang B, Ding Q H, Joseph P V. 2009. Objective definition of the Indian summer monsoon onset. J Clim, 22: 3303–3316
Wu G X, Zhang Y S. 1998. Tibetan Plateau forcing and the timing of the monsoon onset over South Asia and the South China Sea. Mon Weather Rev, 126: 913–927
Xavier P K, Marzin C, Goswami B N. 2007. An objective definition of the Indian summer monsoon season and a new perspective on the ENSO-monsoon relationship. Q J R Meteorol Soc, 133: 749–764
Yang S, Lau K M, Rao M S. 1996. Precursory signals associated with the interannual variability of the Asian summer monsoon. J Clim, 9: 949–964
Yu Lisan, Jin X Z, Weller R A. 2007. Annual, seasonal, and interannual variability of air-sea heat fluxes in the Indian Ocean. J Clim, 20: 3190–3209
Zhang Y N, Wu G X, Liu Y M, et al. 2014. The effect of asymmetric potential vorticity forcing on the instability of South Asian High and India summer monsoon onset. Sci China Earth Sci, 57: 337–350, doi: 10.1007/s11430-013-4664-8